NeuroImage 134 (2016) 475–485

Contents lists available at ScienceDirect

NeuroImage

journal homepage: www.elsevier.com/locate/ynimg

Structural and functional correlates of motor imagery BCI performance: Insights from the patterns of fronto-parietal attention network

Tao Zhang [a], Tiejun Liu [a,b], Fali Li [a], Mengchen Li [a], Dongbo Liu [a], Rui Zhang [a], Hui He [a], Peiyang Li [a], Jinnan Gong [a], Cheng Luo [a,b], Dezhong Yao [a,b], Peng Xu [a,b,*]

[a] Key Laboratory for NeuroInformation of Ministry of Education, School of Life Science and Technology, University of Electronic Science and Technology of China, Chengdu 610054, China
[b] Center for Information in BioMedicine, University of Electronic Science and Technology of China, Chengdu 610054, China

ARTICLE INFO

Article history:
Received 29 October 2015
Revised 4 March 2016
Accepted 13 April 2016
Available online 19 April 2016

Keywords:
Motor imagery
Fronto-parietal attention network
Cortical thickness
Brain computer interface (BCI)
Centrality
Support vector machine (SVM)

ABSTRACT

Motor imagery (MI)-based brain-computer interfaces (BCIs) have been widely used for rehabilitation of motor abilities and prosthesis control for patients with motor impairments. However, MI-BCI performance exhibits a wide variability across subjects, and the underlying neural mechanism remains unclear. Several studies have demonstrated that both the fronto-parietal attention network (FPAN) and MI are involved in high-level cognitive processes that are crucial for the control of BCIs. Therefore, we hypothesized that the FPAN may play an important role in MI-BCI performance. In our study, we recorded multi-modal datasets consisting of MI electroencephalography (EEG) signals, T1-weighted structural and resting-state functional MRI data for each subject. MI-BCI performance was evaluated using the common spatial pattern to extract the MI features from EEG signals. One cortical structural feature (cortical thickness (CT)) and two measurements (degree centrality (DC) and eigenvector centrality (EC)) of node centrality were derived from the structural and functional MRI data, respectively. Based on the information extracted from the EEG and MRI, a correlation analysis was used to elucidate the relationships between the FPAN and MI-BCI performance. Our results show that the DC of the right ventral intraparietal sulcus, the EC and CT of the left inferior parietal lobe, and the CT of the right dorsolateral prefrontal cortex were significantly associated with MI-BCI performance. Moreover, the receiver operating characteristic analysis and machine learning classification revealed that the EC and CT of the left IPL could effectively predict the low-aptitude BCI users from the high-aptitude BCI users with 83.3% accuracy. Those findings consistently reveal that the individuals who have efficient FPAN would perform better on MI-BCI. Our findings may deepen the understanding of individual variability in MI-BCI performance, and also may provide a new biomarker to predict individual MI-BCI performance.

1. Introduction

Motor imagery (MI) is an internal mental rehearsal of a special motor action without overt motor output, which reflects high-level aspects of action planning. Although this is an abstract description, numerous studies have demonstrated that MI plays a crucial role in motor skill learning, rehabilitation of motor abilities and prosthesis control (Burianova et al. 2013; Miller et al., 2010). Meanwhile, brain computer interface (BCI) approaches hold promise to provide effective treatment for people with motor impairments, such as spinal cord injury (SCI), stroke, and amyotrophic lateral sclerosis (ALS) (Lebedev and Opris, 2015). Moreover, BCIs can be utilized to enhance normal brain function (i.e., sports skills) (Krauledat et al., 2009). Therefore, many recent efforts to develop MI-based BCI systems to obtain voluntary neural electroencephalography (EEG) signals (i.e., sensorimotor rhythm (SMR) or mu rhythm) for the paralyzed patients or healthy individuals, allowing to control external devices and to better understand cognitive behaviors (Alvarez-Meza et al., 2013; Friedrich et al., 2013; Miller et al., 2010).

In real-word BCI applications, there are large inter-individual differences in MI-BCI performance, not all individuals show satisfactory performance. For example, according to a study conducted by Blankertz et al. (2010b), approximately 15% to 30% of subjects cannot successfully voluntarily control an SMR-BCI, even after several weeks of training. In an earlier study published in 2003, the percentage of subjects who achieved a classification accuracy below 70% was even greater (48.7%) (Guger et al., 2003). Therefore, it is important to better understand the reasons for the individual differences in MI-BCI performance and find reliable biomarkers to predict individual MI-BCI performance (Blankertz et al., 2010a). The development of predictors could identify potentially inefficient SMR-BCI subjects, thereby avoiding frustrating

* Corresponding author at: Key Laboratory for NeuroInformation of Ministry of Education, School of Life Science and Technology, University of Electronic Science and Technology of China, Chengdu, China.
E-mail address: xupeng@uestc.edu.cn (P. Xu).

http://dx.doi.org/10.1016/j.neuroimage.2016.04.030
1053-8119/

and costly training procedures. Thus, other studies on this topic may be instructive for the establishment of enhanced training strategies for subjects who exhibit poor performance on these tasks (Vidaurre and Blankertz, 2010).

Due to the rapid development of neuroimaging techniques, such as EEG, functional magnetic resonance imaging (fMRI), and structural MRI (sMRI), the understanding of MI mechanisms has been progressively improving. Using the direct neuro-recording, several studies revealed that the primary motor cortex (M1) and posterior parietal cortex (PPC) are rich sources of MI EEG signals that can be used to control BCIs (Aflalo et al., 2015; Hochberg et al., 2006). Meanwhile, MRI technique is also growing attraction and has gain researchers attention. Based on fMRI, MI-BCI performance has been found to be correlated with the activation of the supplement motor area (SMA) (Halder et al., 2011), premotor-parietal network (Hanakawa et al., 2003) and a large fronto-parietal network (Hetu et al., 2013). Moreover, studies based on sMRI revealed that the gray matter volume of the SMA, supplementary somatosensory area and dorsal premotor cortex (Kasahara et al., 2015) and the fractional anisotropy (FA) of the cingulum, corpus callosum and superior fronto-occipital fascicle (Halder et al., 2013) are closely correlated with MI-BCI performance. These related studies were mainly focused on task-related performance and consistently illustrated the important role of the fronto-parietal regions in MI-BCI performance. Although many efforts (Kasahara et al., 2015; Zich et al., 2015) were paid to understand these patterns, the underlying neural mechanism remains unclear.

In recent years, functional connectivity changes in an intrinsic resting-state brain network (i.e., the fronto-parietal attention network (FPAN) and default mode network (DMN)) and neural structural patterns have been increasingly used to investigate cognitive performance (Alavash et al., 2015; Kasahara et al., 2015; Markett et al., 2014). The FPAN is a task-positive network consisting of the areas of the cortex located along the intraparietal sulcus (IPS), dorsolateral prefrontal cortex (DLPFC), inferior parietal lobe (IPL), SMA, and frontal eye field (FEF) (Fox et al., 2005; Ptak, 2012) that is crucially involved in high-level cognitive processes, such as attention and working memory (Markett et al., 2014; Naghavi and Nyberg, 2005; Ptak, 2012; Scolari et al., 2015). Studies have also suggested that MI has a critical functional relationship with these high-level cognitive processes (Ashley Fox, 2013; Madan and Singhal, 2012). Sustained attention and working memory are two crucial factors for healthy subjects to successfully control an MI-based BCI, and general mind wandering or lapses in attention can undermine the user's efforts in performing this task (Friedrich et al., 2013; Lakey et al., 2011). These studies imply that MI-BCI performance relies on the interactions between high-level cognitive and low-level motor functions (Lebedev and Opris, 2015; Moxon and Foffani, 2015). Thus, in the current study we combined EEG and MRI to characterize the relationships between the FPAN and MI-BCI performance.

Functional and structural MRI may offer two complementary sources of information to facilitate an understanding of the relationships between the FPAN and MI-BCI performance. First, the graph tool from network analysis is an important method for capturing the intrinsic functional organization of the brain, which typically reflects the exchange of information (integration and segregation) among brain regions (Sporns, 2013b; Tuladhar et al., 2015). In a functional brain network, the hub plays a critical role in information processing and translation by altering its functional connectivity with other nodes (brain regions) within the network to modulate the various cognitive processes (Cole et al., 2013; Zanto and Gazzaley, 2013). Insults to a hub of a network will result in a disproportionately high impact on behavior or severe cognitive impairment (Osada et al., 2015). A variety of methods allow for the characterization of the importance or 'hubness' of a node in the network, and each measure seems to reflect unique network patterns (Sporns, 2013b; Zuo et al., 2012). Here, the degree centrality (DC) and eigenvector centrality (EC), two common centrality measurements, were selected to assess the network properties of the FPAN (Lohmann et al., 2010; Sato et al., 2015). Second, measurement of the cortical thickness (CT) is other important method to capture the cortical morphology feature of the brain. CT reflects cellular characteristics, such as myelination, cell size, and cell packing density (Lerch et al., 2006; Narr et al., 2007). Several studies have assessed cognitive ability in healthy subjects or in populations with mental disorders using the changes of CT that typically may reflect structural reorganization (local alterations or network-level modulations) (Voss and Zatorre, 2015; Zielinski et al., 2014). Thus, the combination of regional CT and functional network hub (DC and EC) evaluations may provide new insights into the associations between the FPAN and MI-BCI performance.

We hypothesized that determining the specific patterns of FPAN organization, as reflected by the resting-state functional network and the regional morphometric changes in cortical structural, would facilitate our understanding of the individual differences in MI-BCI performance. We also hypothesized that these functional and structural patterns of the FPAN could be used to predict individual MI-BCI performance. Therefore, in the present study, we assessed the structural and functional patterns of the FPAN at the node level. Specifically, we examined one structural measure (CT) and two resting-state functional network node-centrality measures (DC and EC). Based on these functional and structural measurements, we assessed the effects of different patterns of the organization of the FPAN on individual MI-BCI performance using a correlation analysis and a receiver operating characteristic (ROC) analysis. Linear discriminant analysis (LDA) and support vector machine (SVM) classifiers were then used to identify subjects with poor MI-BCI performance.

2. Materials and methods

2.1. Subjects

A total of 40 healthy university students were initially recruited, and 26 (9 females and 17 males, aged 22.85 ± 2.48 years, range 19–26 years, 24 right hand-dominant) agreed to complete the EEG and MRI recordings. The subjects did not habitually consume drugs and alcohol, and had no cognitive impairments or neurological disorders. Two subjects had previous experience with MI-based BCI. The experimental protocol was approved by the Institutional Research Ethics Board of the University of Electronic Science and Technology of China (UESTC). All participants were asked to read and sign an informed consent form before participating in the study. After the experiment, all participants received monetary compensation for their time and effort.

2.2. EEG data acquisition

EEG data were recorded using a Symtop amplifier (Symtop Instrument, Beijing, China) with 15 Ag/AgCl electrodes (F3, F4, FC3, FC4, Cz, C3, C4, C5, C6, CP3, CP4, P3, P4, O1, O2) from an extended 10–20 system. The AFz electrode was adopted as the reference, and the signals were sampled at 1000 Hz and filtered with a band-pass filter between 0.5 and 45 Hz.

2.3. Experimental procedure

At the beginning of the study, all subjects were told that the purpose of the study was to investigate individual variability in controlling an MI-based BCI. The subjects were then familiarized with the experimental paradigm as shown in Fig. 1. Specifically, the participants were instructed to use kinesthetic rather than visual imagery (Neuper et al., 2005). To achieve reliable MI-BCI performance, the EEG experimental datasets consisted of two sessions. All 40 subjects participated in the first session. Twenty-six subjects returned to participate in the second session. The mean interval between the two sessions was approximately 3 months (95 ± 8 days), and the same tasks were performed

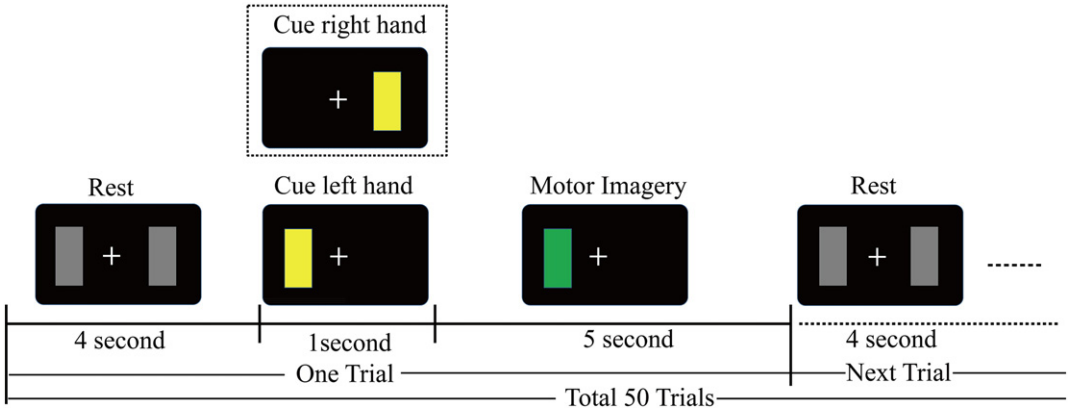

Fig. 1. BCI experimental paradigm. Offline experimental procedures and duration for one left/right hand trail, consisting of a 4 s rest period, indicated by gray bars on both sides; a 1 s cue, indicated by a yellow bar on the left/right side; and a 5 s MI task, indicated by a green bar on the left/right side.

in each session. For each session, all measurements from one participant were recorded on the same day.

Each EEG session consisted of four runs, and each run consisted of 50 trials comprising approximately 25 trials for each MI condition (left or right hand). A break of 2 min was given to allow the subjects to rest between the two consecutive runs. In total, each subject performed 200 MI trials. Each trail began with a 4 s rest period. A yellow bar then appeared on the left or right side of the screen for 1 s to instruct the subjects to perform the left or right hand MI task. When the yellow bar turned green, the subjects performed the requested MI task for 5 s (see Fig. 1).

2.4. MRI data acquisition

The 26 subjects who completed both EEG experiments were further asked to participate in MRI scanning. Images were acquired on a 3.0 T MRI scanner (GE DISCOVERY MR750, USA) using an eight channel-phased array head coil. Functional images were collected by a single-shot, gradient recalled echo-planar imaging (EPI) sequences (TR = 2000 ms, TE = 30 ms, flip angle = 90°, matrix size = 64 × 64, field of view (FOV) = 24 × 24 cm^2, slice thickness/gap = 4 mm/0.4 mm, and 32 slices oriented in an AC-PC line). All subjects underwent an 8.5 min resting fMRI scan. During the resting state fMRI scan, participates were instructed to hold still, close their eyes, and relax their minds. High-resolution T1-weighted images were acquired by using a-dimensional fast spoiled gradient echo (T1-3D FSPGR) sequence (TR = 5.96 ms, TE = 1.968 ms, flip angle = 9°, matrix size = 256 × 256, FOV = 25.6 × 20.5 cm^2, and slice thickness (no gap) = 1 mm).

2.5. Analysis procedure

A block diagram of the data analysis procedure is shown in Fig. 2. The raw EEG, fMRI, and sMRI data were first preprocessed. Then, the preprocessed datasets were analyzed. The MI EEG data were used to evaluate MI-BCI performance. Based on graph-theory techniques, we constructed a weighted graph for the FPAN using the resting state fMRI and then extracted the weighted DC and EC for each node of the FPAN. We also extracted the CT of the corresponding regions (nodes) within the FPAN using the sMRI data. Finally, the associations between the FPAN and MI-BCI performance were assessed using Pearson's correlation. We used the results to determine whether the observed structural and functional features could accurately differentiate the low-aptitude BCI group from the high-aptitude BCI group based on ROC analysis and on LDA and SVM classification. The details of those steps are described in the following sections.

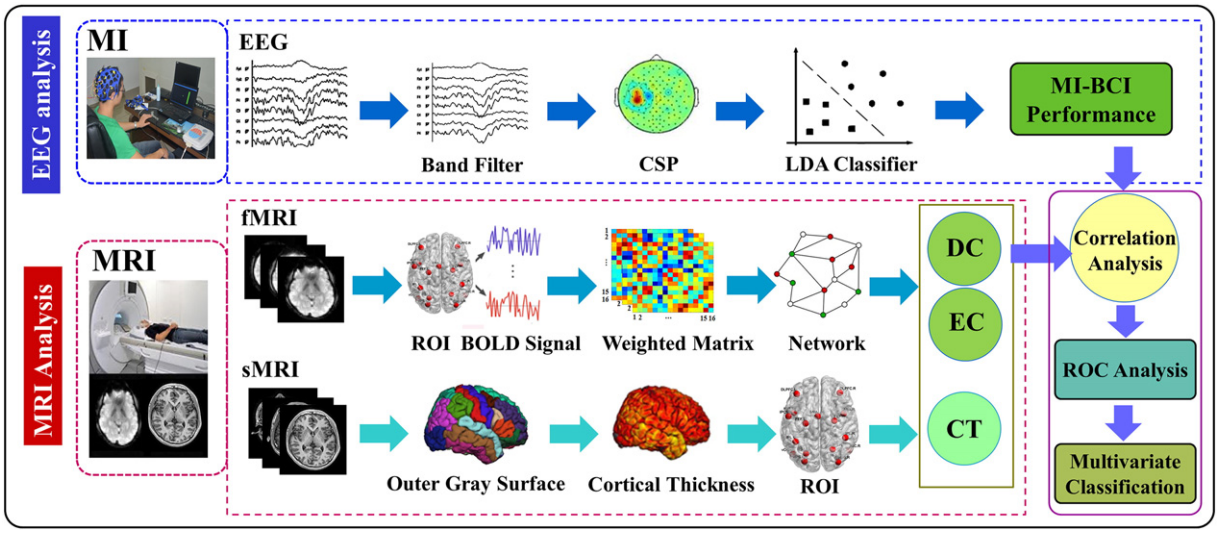

Fig. 2. The analysis procedure.

2.6. MI-BCI performance

The trials with an absolute amplitude exceeding 100 μv were discarded (Kasahara et al., 2015; Zhang et al., 2015a). For each experimental EEG session, we used the first 2 runs of the EEG dataset as the training set and the last 2 runs as the testing set. The aim of the training set was to estimate the subject dependent parameters, such as the band-pass filter and the common spatial pattern (CSP) spatial filters, and then use these to train the corresponding classifier model. Based on these parameters and the classifier model determined by the training set, MI-BCI performance was estimated using the testing sets.

Based on the trials in training set, the subject-specific optimal band-pass filter can be determined by r^2 as shown below (McFarland et al., 1997; Xu et al., 2011),

$$r^2 = \left(\frac{\sqrt{L_1 L_2}}{L_1 + L_2}\frac{\mathrm{mean}(X_1) - \mathrm{mean}(X_2)}{\mathrm{std}(X_1 \cup X_2)}\right)^2 \quad (1)$$

where X_1 and X_2 are the task related power spectrum of the two classes, L_1 and L_2 are the number of trials in the two corresponding classes, and r^2 represents the power differences between two classes. The band-pass filter corresponding to the largest r^2 was treated as the optimal band-pass filter for the current subject, and was used to filter both the training and testing sets. Then, three pairs of optimal spatial filters were estimated by CSP based on the band-pass filtered training EEG signals for each subject (Li et al., 2013; Muller-Gerking et al., 1999; Zhang et al., 2013b). The logarithm transformation of the variance of the spatially filtered signals, resulting in a 6-dimensional CSP feature vector, served as training features. Considering the heteroscedastic distribution situation usually encountered in an MI BCI system, Z-score linear discriminate analysis (Z-LDA) was used as the classifier for the recognition of tasks (left or right MI) (Zhang et al., 2013a). The Z-score is an enhanced version of LDA which identifies a decision boundary based on the Z-score that utilizes both the mean and standard deviation of the projected data to adaptively adjust the decision boundary to fit a heteroscedastic distribution situation (Zhang et al., 2013a).

For the testing process, the same band-pass and spatial CSP filters determined from the training process were used to filter the trials from the testing set. Then, the 6-dimensional log-variance of the filtered EEG signal was estimated for each trial, and the trained Z-LDA classifier performed the recognition task by inputting the 6-dimentional testing CSP feature. The mean accuracies of the two EEG sessions in the testing set were regarded as the measure of MI-BCI performance for all subjects (Zhang et al., 2015a).

2.7. fMRI data processing

For each participant, the first five volumes were initially discarded to ensure magnetization equilibrium. Then, the remaining functional scans were slice time corrected, 3D head motion corrected, spatially normalized ($3 \times 3 \times 3$ mm^3), and spatially smoothed (8 mm full-width at half maximum Gaussian kernel) in SPM8 software package. Participants with head motion less than ± 1.5 mm in the x, y, or z direction and less than $\pm 1.5°$ rotation in each axis were included. Next, temporally band-pass filtering (0.01–0.08 Hz) was employed to reduce the effects of low-frequency drift and high-frequency physiological noises. To further remove several spurious sources of variance, the filtered time series were regressed out the six head motion parameters, white matter signals, cerebrospinal fluid and whole brain signals.

2.8. Measurement of cortical thickness

The T1-weighted images were processed using the Free-Surfer image analysis suite v5.0.4 (http://surfer.nmr.mgh.havard.edu) to generate a cortical surface model that provided a measure of cortical thickness (Dale et al., 1999). The processing details have been described previously (Han et al., 2006; Kuperberg et al., 2003). Briefly, the automated morphometric procedures included normalization, spatial transforms, tissue segmentation, and surface tessellation. Cortical thickness was quantified at each surface location or vertex as the shortest distance from the white surface to the pial surface (Li et al., 2014). Following surface extraction, sulcal and gyral features across individual subjects were aligned by morphing each subject's brain to an average spherical representation, which allows accurate matching of cortical thickness measurement locations among participants, while minimizing metric distortion. For the whole brain analysis, thickness data were smoothed on the tessellated surfaces using a 20-mm full-with-at-half-maximum Gaussian kernel prior to statistical analysis. Selecting a surface-based kernel reduces measurement noise but preserves the capacity for anatomical localization, as it respects the cortical topological features (Bernhardt et al., 2014). The data quality of the native space cortical thickness images was controlled by visual inspection to avoid aberrations in the estimates of cortical thickness.

2.9. Region of interests

In previous studies (Fox et al., 2005; Markett et al., 2014; Toro et al., 2008), different groups have consistently found sixteen independent regions of interest (ROIs) that could delineate the FPAN. Here, we obtained 16 ROIs (Table 1) according to the coordinates that were reported in these studies and converted them to MNI coordinates. In the resting-state fMRI, we defined 6-mm-radius spheres around these MNI coordinates as the ROI and then the averaged the BOLD time series across the 33 voxels within each ROI, which was used to construct the brain's functional network. For the sMRI data, we followed previously described procedures to extract the regional cortical thickness of each node within the FPAN (Bernhardt et al., 2014; Sowell et al., 2004).

2.10. Weighted graph construction of the FPAN

A network typically modeled by graph theory includes a collection of nodes (brain regions) and edges. In this study, we set the ROIs shown in Table 1 as the nodes. Then, the averaged time series of each node was extracted to calculate a correlation matrix using Pearson's correlation. The correlation coefficients between nodes were set as the edges. To observe the topological properties of the network, we constructed a weighted graph for the FPAN. Because calculation of the centrality indexes requires entries to have the same sign (Markett et al., 2014; Sporns, 2013a), edges with negative correlations were set to zero. Finally, a weighted and undirected adjacency matrix (correlation matrix) was obtained for each subject. The EC and DC values were extracted for

Table 1
MNI coordinates and Brodmann area of the 16 ROIs in the FPAN.

Brain regions	Brodmann	MNI coordinates		
		x	y	z
L dorsal intraparietal sulcus (L.dIPS)	7	−23	−70	46
R dorsal intraparietal sulcus (R.dIPS)	7	25	−62	53
L inferior parietal lobule (L.IPL)	7	−42	−48	51
R inferior parietal lobule (R.IPL)	40	48	−41	54
L ventral intraparietal sulcus (L.vIPS)	19	−26	−84	24
R ventral intraparietal sulcus (R.vIPS)	19	35	−85	27
L fontal eye field (L.FEF)	6	−24	−15	66
R fontal eye field (R.FEF)	6	28	−10	58
Inferior precentral sulcus (IPCS)	6	−55	−2	38
Supplementary motor area (SMA)	2	−2	−2	55
L dorsolateral prefrontal cortex (L.DLPFC)	46	−40	39	30
R dorsolateral prefrontal cortex (R.DLPFC)	46	38	41	26
L ventral occipital lobe (L.vOC)	53	−47	−71	−8
R ventral occipital lobe (R.vOC)	54	55	−64	−13
L anterior insula (L.aIns)	19	−45	5	9
R anterior insula (R.aIns)	19	45	3	15

Table 2
Descriptive statistics of participants who fully completed the EEG and fMRI experiments. LH (RH) represents left (right) handedness. An invalid session indicates that the subject had excessive head motion during the resting-state fMRI scanning. High-aptitude MI-BCI users are marked with an asterisk (*) in the corresponding column. LA (HA) represents low- (high)-aptitude BCI users.

Subject	Male/female	Age (years)	LH (RH)	MI-BCI performance (%)	High-aptitude	Invalid session
Sub-01	M	26	RH	92	*	No
Sub-02	F	24	RH	66		No
Sub-03	F	24	RH	99	*	No
Sub-04	F	24	RH	70		No
Sub-05	M	23	RH	80	*	No
Sub-06	F	26	RH	80	*	No
Sub-07	M	19	RH	74		No
Sub-08	F	22	RH	82	*	No
Sub-09	M	23	RH	78		No
Sub-10	M	24	LH	78		No
Sub-11	M	24	RH	86	*	No
Sub-12	M	22	RH	85		Yes
Sub-13	F	24	RH	79	*	No
Sub-14	F	22	RH	78		No
Sub-15	M	25	RH	96		Yes
Sub-16	M	19	RH	92	*	No
Sub-17	M	20	RH	56		No
Sub-18	F	26	RH	61		No
Sub-19	M	23	RH	77		No
Sub-20	M	22	RH	57		No
Sub-21	M	22	RH	58		Yes
Sub-22	M	23	RH	58		No
Sub-23	M	20	RH	85	*	No
Sub-24	F	21	RH	52		No
Sub-25	M	24	LH	79	*	No
Sub-26	M	25	RH	93	*	No
Sums	26(17 M/9F)	–	26(24RH/2LH)	–	23(9LA/11HA)	–
Mean	–	22.8 ± 2.48	–	–	–	–
Median	–	–	–	78	–	–
Range	–	19–26	–	52–99	(52–77)/(79–99)	–

each region within the FPAN based on the weighted and undirected adjacency matrix using the Brain Connectivity Toolbox (Rubinov and Sporns, 2010).

2.11. Weighted graph metric definitions

2.11.1. Degree centrality

Degree centrality (DC) is defined as the sum of all neighboring link weights (sometimes referred to as the strength) (Rubinov and Sporns, 2010). If a node has strong connections to many other nodes in the network, then the DC for this node is high. The DC describes local directed connectivity relationships which can be computed as follows:

$$\mathrm{DC}(i) = \sum_{j=1}^{N} a_{ij} \tag{2}$$

where N is the number of nodes in the network, and a_{ij} is the connection strength between node i and node j.

2.11.2. Eigenvector centrality

Eigenvector centrality (EC) is defined as the first eigenvector of the adjacency matrix, which corresponds to the largest eigenvalue λ_1 (i.e., the principal eigenvalue). EC is calculated as follows:

$$\mathrm{EC}(i) = \mu_1(i) = \frac{1}{\lambda_1} A\mu_1 \tag{3}$$

where A is the adjacency matrix of the graph, μ_1 is the eigenvector, and λ_1 is the eigenvalue. Because of the recursive property of this calculation, a high EC for a node means that are themselves highly connected (Thomas et al., 2015; Zuo et al., 2012). Compared to the DC, the EC reflects the global hierarchical relevance of a node within the network. Thus, when a node with high EC (i.e., more central) is damaged or 'infected', there is a greater impact on the network's efficiency or functional performance (Thomas et al., 2015).

2.12. Correlation analysis

The major focus of the current investigation was to explore the relationships between the functional and structural features of the FPAN and MI-BCI performance. For each subject, we extracted the resting-state functional network properties (DC and EC) and a regional cortical structural feature (CT) for each ROI within the FPAN. Pearson's correlation was then performed to assess the relationships between the structural and functional features of the FPAN and MI-BCI performance.

2.13. Categorization into low- and high-aptitude users

Two steps were needed to classify the subjects into the two groups. The first step was the selection of critical features with good discriminative abilities. The second step was to perform the classification based on the selected features in the first step. In the pattern recognition community, a ROC curve is one of the most common criteria used to evaluate the classification ability of a feature.

A ROC curve is a plot of the false positive rate (FPR) against the true positive rate (TPR), which is generated by varying the range of discrimination thresholds (Fawcett, 2006; Zalesky et al., 2010). An ideal point would be located in the upper left corner of the ROC curve, which represents 100% sensitivity and 100% specificity. Regarding the ROC, the area under the curve (AUC) is typically used to quantify the classification ability of a feature, and a large AUC indicates a strong classification ability of a feature. In the present study, a ROC analysis was performed using all subjects.

Based on the ROC analysis, the features with a strong discriminative ability (i.e., a large AUC) can be determined. Therefore, by concatenating the selected features, we further evaluated the possibility of classifying the participants into high- and low-aptitude BCI users using both LDA and a radial basis function (RBF) kernel SVM classifier which was implemented using the LIBSVM toolbox (Chang and Lin, 2011; Liu et al., 2013a). The classifier performance was validated using a leave-one-out cross validation (LOOCV) strategy. Specifically, for n samples, in

Table 3
Correlation between node centrality measures of FPAN topology, regional cortical thickness, and MI-BCI performance.

	DC vs. BCI performance[a]		EC vs. BCI performance[a]		CT vs. BCI performance[b]	
	r	p-value	r	p-value	r	p-value
L.dIPS	0.3075	0.1535	−0.3118	0.1474	0.1658	0.4997
R.dIPS	0.1868	0.3933	0.1175	0.5934	−0.1187	0.5895
L.IPL	−0.1327	0.5462	**−0.5048**	**0.0140**	**−0.4155**	**0.0486**
R.IPL	−0.1415	0.5197	0.3580	0.0935	−0.2603	0.2303
L.vIPS	0.3571	0.0944	−0.2917	0.1768	−0.2894	0.1805
R.vIPS	**0.4378**	**0.0367**	−0.3103	0.1496	−0.1413	0.5201
L.FEF	−0.1306	0.5527	−0.0078	0.9718	−0.2871	0.1841
R.FEF	−0.0387	0.8608	−0.0065	0.9766	−0.3454	0.1065
L.iPCS	−0.1681	0.4433	0.0211	0.9237	0.0996	0.6513
SMA	−0.1176	0.5932	−0.1492	0.4967	−0.2820	0.1924
L.DLPFC	−0.1702	0.4374	0.2468	0.2563	−0.0634	0.7737
R.DLPFC	0.0521	0.8135	0.3839	0.0705	**−0.5890**	**0.0031**
L.vOC	0.1841	0.4005	−0.1091	0.6200	−0.0430	0.8456
R.vOC	0.2271	0.2974	0.0345	0.8757	−0.0400	0.8562
L.aIns	0.0193	0.9303	−0.1462	0.5057	−0.0798	0.7175
R.aIns	0.2889	0.1811	−0.0124	0.9552	0.0565	0.7979

A bold value indicates statistical significance ($p < 0.05$).
[a] Correlation between node centrality and MI-BCI performance.
[b] Correlation between regional (node) CT and MI-BCI performance.

each LOOCV test, n-1 samples were chosen for training, and the remaining one sample was used for testing. This procedure was repeated n times until all samples had served as the testing set. Regarding the optimal values for the RBF kernel parameters C and γ, we performed another nested LOOCV on the training set (i.e. n-1 samples), which will result in the corresponding optimized C and γ for each training set. Then the SVM classifier will be trained by applying the optimized parameters to the training set, based on which the testing set will be finally classified (Chang and Lin, 2011; Kothari et al., 2013; Liu et al., 2013b).

3. Results

3.1. MI-BCI offline performance

Of the 26 subjects who fully completed the EEG and fMRI recordings in the study, three subjects were excluded due to excessive motion during resting-state fMRI scanning. Table 2 list a detailed overview of all subjects. The MI-BCI performances were used to divide the subjects into low- and high-aptitude groups. Following the criteria proposed in the Halder studies (Halder et al., 2011; Halder et al., 2013), the median performance value (78%) was used to separate the subjects into good and poor performance groups. To prevent possible overlap between the two groups, 3 subjects with 78% accuracy were excluded. This resulted in nine low- and 11 high-aptitude BCI users as the two groups.

3.2. Node centrality and MI-BCI performance

Table 3 summarizes all correlation analysis results between node centrality and MI-BCI performance (Table 3a). We found that MI-BCI performance was positively correlated ($r = 0.4378$, $p = 0.0367$) with the DC of the right ventral intraparietal sulcus (vIPS, $x = 35$, $y = -85$, $z = 27$) (Fig. 3a), but negatively correlated ($r = -0.5048$, $p = 0.0140$) with the EC of the left inferior parietal lobule (IPL, $x = -42$, $y = -48$, $z = 51$) (Fig. 4a). Analysis of differences between the low- and high-aptitude groups revealed a significantly lower DC of the right vIPS and a higher EC of the left IPL for the low-aptitude group (Wilcoxon rank sum test, low-aptitude users $n = 9$, high-aptitude users $n = 11$, $p < 0.05$) (Fig. 3b and Fig. 4b).

3.3. Regional cortical thickness and MI-BCI performance

Table 3 also summarizes up all the correlation analysis results between the regional (node) CT and MI-BCI performance (Table 3b). We found that MI-BCI performance was negatively correlated with the CT of both the left inferior parietal lobule (IPL, $x = -42$, $y = -48$, $z = 51$) (Fig. 4c) and the right dorsolateral prefrontal cortex (DLPFC, $x = 38$, $y = 41$, $z = 26$) (Fig. 5a). Analysis of the differences between the low- and high-aptitude groups revealed a significantly greater CT of the left IPL in the low-aptitude group (Fig. 4d), while no significant difference was observed in CT of the right DLPFC (Fig. 5b) (Wilcoxon rank sum test, low-aptitude users $n = 9$, high-aptitude users $n = 11$, $p < 0.05$).

3.4. Classification of the two groups

As revealed in Fig. 6, the ROC analysis demonstrates that the EC and CT of the left IPL have good classification capabilities with AUC values of 0.82 and 0.81, respectively. To further evaluate the classification capability of the left IPL, we constructed a multivariate feature by concatenating the EC with the CT of the left IPL, generating a two-dimensional feature vector. Fig. 7 shows the scatter plot of this 2-dimensional feature vector for the two groups. In order to obtain relatively robust classification accuracy, we calculated the Mahalanobis distance (Blankertz et al., 2010b; Zhang et al., 2015b) to the data center for each sample. We found that two points marked with green circles in Fig. 7 in the high-aptitude group have greater Mahalanobis distances.

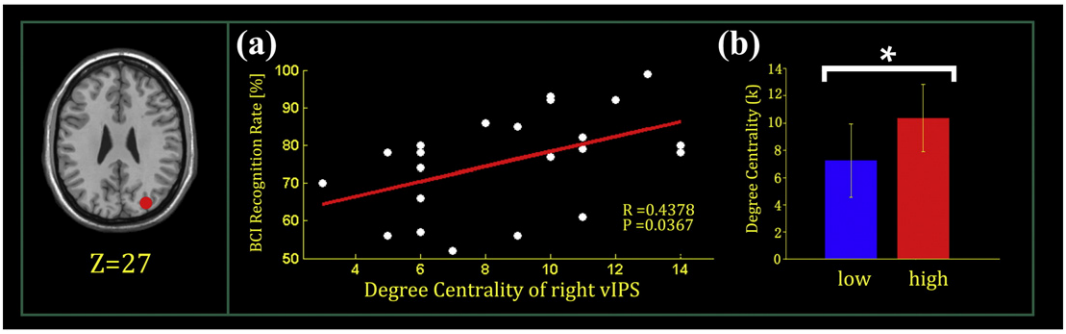

Fig. 3. The relationship between the DC of the right vIPS (x = 35, y = −85, z = 27) and MI-BCI performance. (a) Correlation between the DC of the right vIPS and MI-BCI performance. (b) The difference (means ± SD) between the low-aptitude group (blue bar) and the high-aptitude group (red bar) based on the DC of the right vIPS in the FPAN. The asterisk ('*') denotes a significant difference in the DC of the right vIPS between the two groups.

Applying this technique two points of sample were considered outliers and removed from classification. Table 4 shows that LDA classification achieved an accuracy of 77.8%, a sensitivity of 66.7%, and a specificity of 88.9%. In contrast, the RBF kernel SVM classification achieved an accuracy of 83.3%, a sensitivity of 77.8%, and a specificity of 88.9%. The details of the performance of each classifier are shown in Table 4.

4. Discussion

In the current study, we applied weighted graph measures to understand how specific patterns of FPAN organization (intrinsic functional connectivity) during rest affect individual MI-BCI performance. We also used structural MRI to quantify a specific regional-dependent cortical structural morphometric feature (cortical thickness) within the FPAN to further understand individual variations in MI-BCI performance. Our findings showed that node-level functional or structural changes in three 'core' regions in the FPAN, right vIPS, left IPL, and right DLPFC, were associated with MI-BCI performance.

The FPAN is crucially involved in high-level cognitive processes, such as working memory, attention, and motor function (Markett et al., 2014; Molinari et al., 2013; Neuper et al., 2005; Ptak, 2012). Additionally, the performance of MI has been shown to involve working memory and attention (Ashley Fox, 2013). Extensive evidence indicates that the FPAN plays an important role in MI modulation (Grosse-Wentrup and Schölkopf, 2013; Hetu et al., 2013). Recently, Cole and his colleagues (Cole et al., 2013) showed that the flexible hubs of the fronto-parietal network play a central role in cognitive control and adaptive implementation of the demands of various tasks. However, the individual role of the sub-regions within the FPAN during a specific task state (i.e., motor imagery) are still unknown (Scolari et al., 2015).

Therefore, the present study was done to further understand how functional and structural pattern changes in the FPAN affect inter-individual differences in MI-BCI performance. Using the fMRI, the first centrality measurement we assessed for the FPAN in our study was the DC, which reflects the number and strength of local network connections and also highlights the capacity of a node to catch (i.e., share and propagate stimulus information) local information flowing through

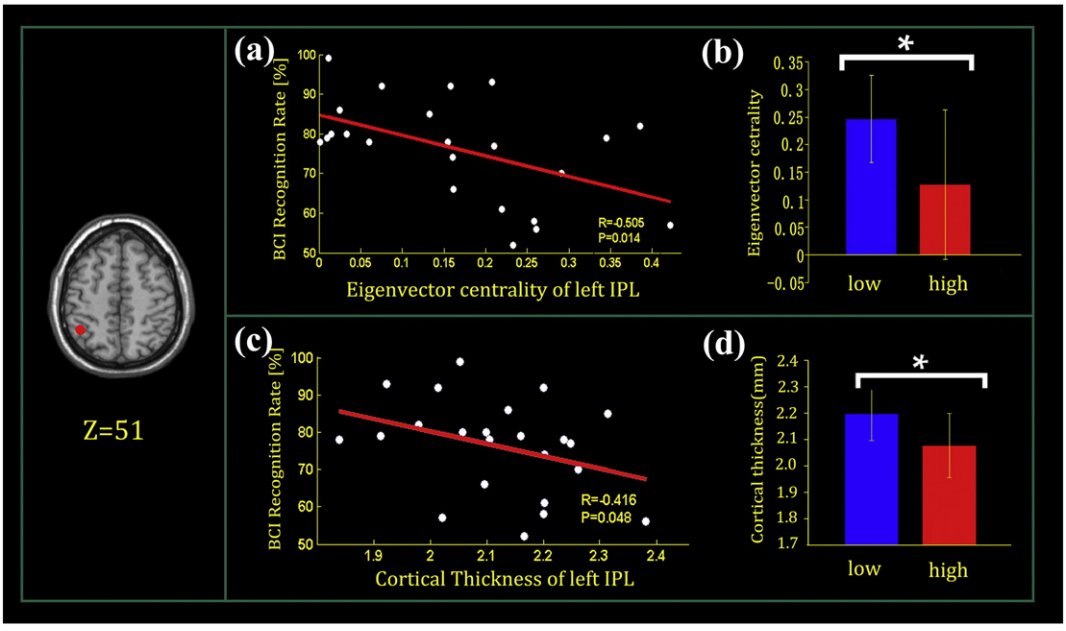

Fig. 4. The relationships between the CT/EC of the left IPL and MI-BCI performance. (a) Correlation between the EC of the left IPL (x = −42, y = −48, z = 51) and MI-BCI performance. (b) The difference (means ± SD) between the low-aptitude group (blue bars) and the high-aptitude group (red bars) based on the EC of the left IPL in the FPAN. (c) Correlation between the CT of the left IPL and MI-BCI performance; (d) The difference (means ± SD) between the low-aptitude group (blue bars) and the high-aptitude group (red bars) based on the CT of the left IPL in the FPAN. The asterisk (*) denotes a significant difference in the EC and CT of the left IPL between the two groups.

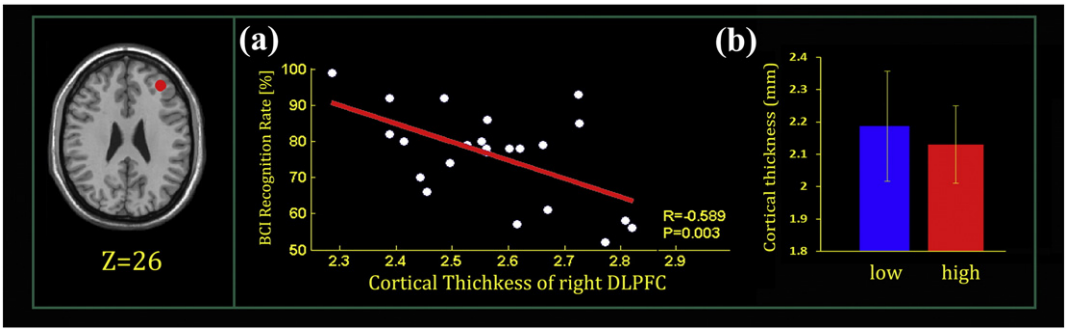

Fig. 5. The relationship between the CT of the right DLPFC (x = 38, y = 41, z = 26) and MI-BCI performance. (a) Correlations between the CT of the right DLPFC and MI-BCI performance; (b) The group difference (mean ± SD) between the low-aptitude group (blue bar) and the high-aptitude group (red bar) according to the CT of the right DLPFC in the FPAN. No significant difference in the CT was observed between the two groups in the right DLPFC.

a network (Borgatti, 2005). A recent graph-theoretical study showed that working memory was significantly positively correlated with the DC, primarily in the bilateral parietal and right superior temporal gyrus and the right insular cortex (Langer et al., 2013). In this study, we found a significant positive correlation ($r = 0.4378$, $p = 0.0367$) between the DC of the right vIPS and MI-BCI performance, and a significant increase in the DC of the right vIPS was observed in subjects who exhibited good MI-BCI performance (see Fig. 3b). Several studies examining both the human and macaque monkey, have determined that the right vIPS is correlated with mental rotations and translations, which are usually involved in the imagery process (Chen et al., 2011; Guipponi et al., 2013; Zacks, 2008). Furthermore, in a recent study, Markett et al. (2014) revealed that the DC of the right vIPS in the resting-state FPAN contributed to alerting and executive functions, two domains of attention. This is consistent with our finding that the DC of the right vIPS is correlated with MI-BCI performance. Similar to previous conclusions (Alavash et al., 2015; Power et al., 2013), our findings suggest that the higher DC in the right vIPS might enhance the direct and efficient information transfer (i.e., sustain attention while ignoring distractors) of the FPAN during MI. In addition to the vIPS, the dorsal IPS was found to be involved in the FPAN. Similar to that of the vIPS, the DC of the left IPS showed a relatively strong positive correlation ($r = 0.3075$, $p = 0.1535$) with MI-BCI performance, although the correlation was not significant. The human IPS region is crucial for processing the signals involved in multisensory attention and is thought to be a site for the top-down control of attention (Anderson et al., 2010). The dorsal and ventral IPS regions have different functional contributions to attentional modalities. Specifically, the brain region around the dorsal IPS shows a more sustained activation during tasks requiring spatial attention, whereas the vIPS is more activated during spatial selection tasks (Corbetta et al., 2002; Corbetta and Shulman, 2002; Hopfinger et al., 2000). Moreover, previous studies have found that the left PPC (mainly the left dIPS region) is activated earlier than the right region during a mental imagery task (Formisano et al., 2002; Luckmann et al., 2014; Sack, 2009; Sack and Schuhmann, 2012).

The second centrality measurement of the FPAN that we evaluated was the EC, which reflects the global association structure of the network and is sensitive to different layers of network hierarchy (Binnewijzend et al., 2014; Lohmann et al., 2010). According to previous studies, a highly associated structure is more vulnerable (i.e., suffers more severe effects on network efficiency) to localized damage to those nodes with high EC values (Bullmore and Sporns, 2009; Osada et al., 2015). Previous work has shown that a stable decrease of EC in the cortex (caudate and parahippocampal cortex) and in non-cortical regions (cerebellum and thalamus) may be associated with the development of the voluntary modulation of behaviors, such as fear and inhibitory control, which are observed in adults (Sato et al., 2015). In our study, we found that the EC of the left IPL showed a significant negative association ($r = -0.5048$, $p = 0.0140$) with MI-BCI performance and a significantly decreased EC of the left IPL was observed in those subjects with good MI-BCI performance (see Fig. 4b). These results

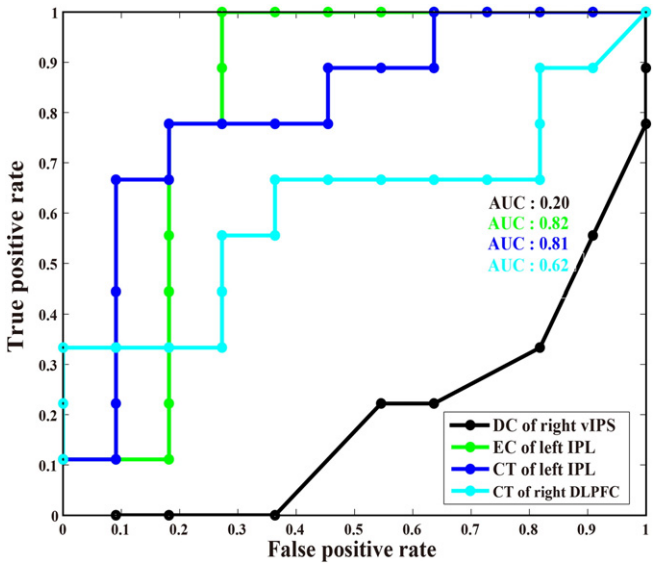

Fig. 6. The ROC curves for the four predictors. The x-axis denotes the false positive rate, and the y-axis denotes the true positive rate. The green line indicates the EC of the left IPL. The dark blue line indicates the CT of the left IPL. The black line indicates the DC of the right vIPS. The bright blue line indicates the CT of the right DLPFC.

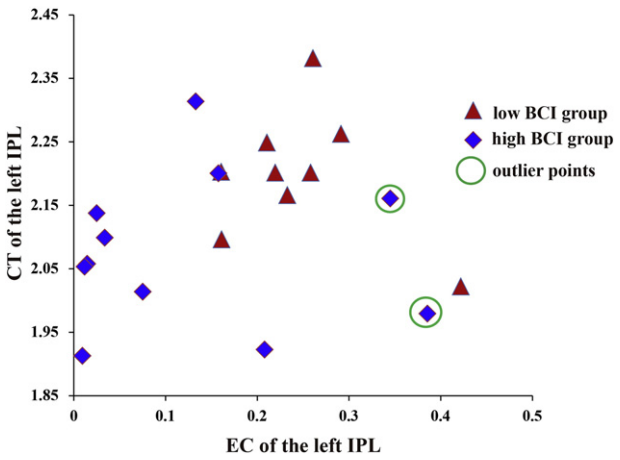

Fig. 7. Scatter plot for the multivariate features of the EC and CT of the left IPL. The blue rhombuses represent the high-aptitude group, and the red triangles represent the low-aptitude group. The green circles denote outlier subjects.

Table 4
Multivariate classification performance for the non-linear SVM and LDA classifiers.

Method	Sensitivity	Specificity	Accuracy
Non-linear SVM	77.8% (7/9)	88.9% (8/9)	83.3% (15/18)
LDA	66.7% (6/9)	88.9% (8/9)	77.8% (14/18)

suggest that the left IPL has a lower hub-like influence on the other nodes of the global FPAN in participants with good MI-BCI performance. However, this finding does not necessarily indicate the left IPL is a brain region with functional disruption. In a recent study, Aflalo et al. presented direct neuro-recording evidence that the PPC, in the left hemisphere, which includes the left IPL, of humans is involved in high-level aspects of action and that the PPC is a rich source of MI EEG signals related to controlling BCIs (Aflalo et al., 2015). Meanwhile, previous studies on other aspects of the PPC found that lesions in the PPC cause deficits in movement rehearsal (Pisella et al., 2000; Sirigu et al., 1996). Using the conditional Granger causality, Gao et al. also revealed that the left IPL serves as the causal source in MI task (Gao et al., 2011). Furthermore, Hetu et al. conducted a meta-analysis on the various types of MI and found that the left IPL was consistently activated during MI of the upper limb, especially during first perspective MI or while imagining more complex movements (Hetu et al., 2013). It is well established that the left IPL is an important hub in MI performance. Thus, we speculated that the decreased EC in the left IPL could be attributed to FPAN reorganization according to the following explanations: The decreased EC might reduce the distraction risk of this node (region) while enhancing the capacity of the individual to resist a disturbance (i.e., maintain sustained attention), and the decreased EC might denote optimized network (FPAN) resource allocation.

Previous studies have shown that MI-BCI performance is correlated with gray matter volume and fractional anisotropy (Halder et al., 2013; Kasahara et al., 2015), but there is no report on the correlation between CT and MI-BCI performance. Structural MRI provided an in vivo proxy of the CT and allowed measurement of the distance from the pial/cortical border to the gray/white matter border (MacDonald et al., 2000; Zhou et al., 2015). CT changes may reflect local functional alterations or global network-level modulations, which have been shown to correlate with cognitive abilities as well as physical and emotional behaviors (Shaw et al., 2013; Voss and Zatorre, 2015; Zhou et al., 2015; Zielinski et al., 2014). Using sMRI, we also extracted the CT of the ROIs within the FPAN to better understand the inter-individual differences in MI-BCI performance. Based on CT analysis, we found a significantly negative correlation ($r = -0.4155$, $p = 0.0486$) between the CT of the left IPL and MI-BCI performance, and a significantly decreased CT of the left IPL was observed for subjects with good MI-BCI performance (see Fig. 4d). Previous studies have found that CT changes are related to high level cognitive abilities, such as working memory and relational thinking (Vendetti and Bunge, 2014). Specifically, cortical thinning has been regarded as a form of the structural reorganization of the cerebral cortex, which is thought to be integral for the functional neural network to enhance the efficiency of information processing (Luna et al., 2010; Zhou et al., 2015). For instance, through the structural function mode, Wendelken has found that cortical thinning in the left IPL leads to greater efficiency in processing first-order relations, thereby reducing dependence on the rostrolateral prefrontal cortex (Wendelken et al., 2011). According to Zielinski et al, there are two possible reasons for cortical thinning: high levels of synapt
ic pruning and a shift in the observed boundary between the gray and white matter (Zielinski et al., 2014). Taking into account both the functional and structural pattern changes of the left IPL, it is plausible to suggest that the thinner CT of the left IPL in better-performing subjects might facilitate improvements in its neural efficiency and the modulation of the FPAN configuration to process the related MI task.

Moreover, the DLPFC is known to participate in executive functions, such as the allocation of attentional resources, performance monitoring, working memory, and response selection, which are thought to play supporting roles for cognitively demanding tasks (Hampshire et al., 2011; Vendetti and Bunge, 2014; Wendelken et al., 2008). Previous studies have indicated that the right DLPFC is associated with movement planning (Halder et al., 2011; Pochon et al., 2001). Additionally, it has been found that the right DLPFC has a stronger activation scale when performing tasks requiring the monitoring function (Sharp et al., 2004). Similar to the left IPL, we found a significant negative correlation ($r = -0.5890$, $p = 0.0031$) between the CT of the right DLPFC and MI-BCI performance. However, no significant difference was found between the two groups in the CT of the right DLPFC (Fig. 5b). We speculate that the reason for this is that the thinner CT of right DLPFC enhances the efficiency of the local neural region during information processing but does not modulate network configuration as strongly as the left IPL, which may account for the fact that we did not observe significant correlations between the DC and EC of the right DLPFC and MI-BCI performance (see Table 3). Therefore, we suggest that the thinner CT in the right DLPFC might also facilitate neural efficiency in processing specific aspects of MI tasks such as guiding and monitoring (Halder et al., 2011; Kuhn et al., 2014).

Furthermore, to further explore the relationship between the FPAN and MI-BCI performance. The subjects were divided into high- and low-aptitude groups according to their MI-BCI performance. Using the ROC analysis, we found that the reduced EC and CT of the left IPL in the FPAN separated the low-aptitude BCI users from the high-aptitude BCI users with a larger AUC. In addition, when we concatenated these two features (EC and CT) of the left IPL as a multivariate predictor (the scatter plot in Fig. 7), the classification accuracy rates were 77.8% and 83.33% using LDA and a SVM as classifiers, respectively, where the two outliers in the high-aptitude BCI group were removed. In this study, because of the small sample size, even a small number of 'abnormal' samples may severely influence the classification. Thus, we treated the two subjects who had high EC values in the high-aptitude BCI group as outliers (marked with green circles in Fig. 7), resulting in 9 low-aptitude and 9 high-aptitude BCI users. The balanced of sample size of the two groups was useful for reducing classification deviation (Japkowicz and Stephen, 2002; Pereira et al., 2009). Although a small sample size was used, our findings provide preliminarily evidence that features of the left IPL can be considered as new biomarkers for predicting individual MI-BCI performance.

Several methodological considerations and limitations of the present study should be mentioned. Due to the long duration of our experiment (approximately 3 months), it was difficult to recruit a large number of subjects, and therefore the current sample size is relatively small. Future studies with imaging data from more subjects will be necessary to confirm our preliminary results. The subjects in the current study were divided into high- and low-aptitude groups according to their MI-BCI performance utilizing the criteria proposed in (Halder et al., 2011). In fact, there may exist more than two groups, such as the low, medium and high performance groups. In the future studies, if the subject number is large enough, we will perform more accurate group divisions to reveal the different neural mechanism among those subjects with different BCI performances. Although it has been shown that the frontoparietal network serves as a flexible hub among the networks used to coordinate the various brain's processes (Zanto and Gazzaley, 2013), self-configuration of the network is still important for supporting cognitive efficiency (Fornito et al., 2013). Thus, we focused on the functional and structural patterns of a single FPAN, which may also provide novel insights for understanding the individual differences in MI-BCI performance. Future studies based on whole-brain or voxel-wise node definition methods need to be performed, which may provide the new insights into the mechanisms of MI from a global large-scale network perspective (Thomas et al., 2015). In addition, in the present study, only two common centrality metrics (DC and EC) were used to measure the properties of the undirected weighted resting-state functional network. Future studies on the effective connectivity and the time-

varying connectivity will be considered to better understand the individual differences in MI-BCI performance (Calhoun et al., 2014).

5. Conclusions

In this study, we found that the structural and functional patterns of the FPAN are associated with MI-BCI performance. Our findings revealed that the individuals who have efficient FPAN would perform better on MI-BCI. Moreover, combining the structural and functional features (i.e., EC and CT of the left IPL) of the FPAN, we were able to accurately identify individuals as low- or high-aptitude BCI users using the machine learning method. Therefore, our study will be helpful for improving our understanding of individual differences in MI-BCI performance. Advancing our understanding of BCI performance in relation to its structural and functional correlate may enable better customization of BCI systems, and be potentially useful for future studies in real-world applications, specifically in BCI control and BCI-based motor function recovery. For instance, first, the study may provide a new biomarker to predict individual MI-BCI performance that can be used to select potential subjects for BCI control and avoid the undesired waste of time necessary for the long training times and the subject frustration associated with these studies. Second, a new rehabilitation strategy using BCI-based motor function recovery could be established where the features of the FPAN may serve as an instructive guide for the design of rehabilitation tasks and BCI systems.

Conflict of interest

None.

Acknowledgements

This work was supported in part by grants from the National Natural Science Foundation of China (# 61522105, # 61175117, # 81330032), the program for New Century Excellent Talents in University (# NCET-12-0089), the 863 Project (# 2012AA011601), and the National Science & Technology Pillar Program (# 2012BAI16B02).

References

Aflalo, T., Kellis, S., Klaes, C., Lee, B., Shi, Y., Pejsa, K., Shanfield, K., Hayes-Jackson, S., Aisen, M., Heck, C., Liu, C., Andersen, R.A., 2015. Neurophysiology. Decoding motor imagery from the posterior parietal cortex of a tetraplegic human. Science 348, 906–910.

Alavash, M., Doebler, P., Holling, H., Thiel, C.M., Giessing, C., 2015. Is functional integration of resting state brain networks an unspecific biomarker for working memory performance? NeuroImage 108, 182–193.

Alvarez-Meza, A.M., Velasquez-Martinez, L.F., Castellanos-Dominguez, G., 2013. Feature relevance analysis supporting automatic motor imagery discrimination in EEG based BCI systems. Conf. Proc. IEEE Eng. Med. Biol. Soc. 2013, 7068–7071.

Anderson, J.S., Ferguson, M.A., Lopez-Larson, M., Yurgelun-Todd, D., 2010. Topographic maps of multisensory attention. Proc. Natl. Acad. Sci. U. S. A. 107, 20110–20114.

Ashley Fox, C.G., 2013. Using motor imagery therapy to improve movement efficiency and reduce fall injury risk. J. Nov. Physiother. 03.

Bernhardt, B.C., Valk, S.L., Silani, G., Bird, G., Frith, U., Singer, T., 2014. Selective disruption of sociocognitive structural brain networks in autism and alexithymia. Cereb. Cortex 24, 3258–3267.

Binnewijzend, M.A.A., Adriaanse, S.M., Van der Flier, W.M., Teunissen, C.E., de Munck, J.C., Stam, C.J., Scheltens, P., van Berckel, B.N.M., Barkhof, F., Wink, A.M., 2014. Brain network alterations in Alzheimer's disease measured by eigenvector centrality in fMRI are related to cognition and CSF biomarkers. Hum. Brain Mapp. 35, 2383–2393.

Blankertz, B., Sannelli, C., Halder, S., Hammer, E.M., Kübler, A., Müller, K.-R., Curio, G., Dickhaus, T., 2010a. Neurophysiological predictor of SMR-based BCI performance. NeuroImage 51, 1303–1309.

Blankertz, B., Sannelli, C., Halder, S., Hammer, E.M., Kubler, A., Muller, K.R., Curio, G., Dickhaus, T., 2010b. Neurophysiological predictor of SMR-based BCI performance. NeuroImage 51, 1303–1309.

Borgatti, S.P., 2005. Centrality and network flow. Soc. Networks 27, 55–71.

Bullmore, E., Sporns, O., 2009. Complex brain networks: graph theoretical analysis of structural and functional systems. Nat. Rev. Neurosci. 10, 186–198.

Burianova, H., Marstaller, L., Sowman, P., Tesan, G., Rich, A.N., Williams, M., Savage, G., Johnson, B.W., 2013. Multimodal functional imaging of motor imagery using a novel paradigm. NeuroImage 71, 50–58.

Calhoun, V.D., Miller, R., Pearlson, G., Adali, T., 2014. The chronnectome: time-varying connectivity networks as the next frontier in fMRI data discovery. Neuron 84, 262–274.

Chang, C.C., Lin, C.J., 2011. LIBSVM: a library for support vector machines. ACM Trans. Intell. Syst. Technol. 2.

Chen, A., DeAngelis, G.C., Angelaki, D.E., 2011. Representation of vestibular and visual cues to self-motion in ventral intraparietal cortex. J. Neurosci. 31, 12036–12052.

Cole, M.W., Reynolds, J.R., Power, J.D., Repovs, G., Anticevic, A., Braver, T.S., 2013. Multi-task connectivity reveals flexible hubs for adaptive task control. Nat. Neurosci. 16, 1348–1355.

Corbetta, M., Shulman, G.L., 2002. Control of goal-directed and stimulus-driven attention in the brain. Nat. Rev. Neurosci. 3, 201–215.

Corbetta, M., Kincade, J.M., Shulman, G.L., 2002. Neural systems for visual orienting and their relationships to spatial working memory. J. Cogn. Neurosci. 14, 508–523.

Dale, A.M., Fischl, B., Sereno, M.I., 1999. Cortical surface-based analysis. I. Segmentation and surface reconstruction. NeuroImage 9, 179–194.

Fawcett, T., 2006. An introduction to ROC analysis. Pattern Recogn. Lett. 27, 861–874.

Formisano, E., Linden, D.E., Di Salle, F., Trojano, L., Esposito, F., Sack, A.T., Grossi, D., Zanella, F.E., Goebel, R., 2002. Tracking the mind's image in the brain I: time-resolved fMRI during visuospatial mental imagery. Neuron 35, 185–194.

Fornito, A., Zalesky, A., Breakspear, M., 2013. Graph analysis of the human connectome: promise, progress, and pitfalls. NeuroImage 80, 426–444.

Fox, M.D., Snyder, A.Z., Vincent, J.L., Corbetta, M., Van Essen, D.C., Raichle, M.E., 2005. The human brain is intrinsically organized into dynamic, anticorrelated functional networks. Proc. Natl. Acad. Sci. U. S. A. 102, 9673–9678.

Friedrich, E.V., Scherer, R., Neuper, C., 2013. Long-term evaluation of a 4-class imagery-based brain-computer interface. Clin. Neurophysiol. 124, 916–927.

Gao, Q., Duan, X., Chen, H., 2011. Evaluation of effective connectivity of motor areas during motor imagery and execution using conditional Granger causality. NeuroImage 54, 1280–1288.

Grosse-Wentrup, M., Schölkopf, B., 2013. A Review of Performance Variations in SMR-Based Brain–Computer Interfaces (BCIs). pp. 39–51.

Guger, C., Edlinger, G., Harkam, W., Niedermayer, I., Pfurtscheller, G., 2003. How many people are able to operate an EEG-based brain-computer interface (BCI)? IEEE Trans. Neural Syst. Rehabil. Eng. 11, 145–147.

Guipponi, O., Wardak, C., Ibarrola, D., Comte, J.C., Sappey-Marinier, D., Pinede, S., Ben Hamed, S., 2013. Multimodal convergence within the intraparietal sulcus of the macaque monkey. J. Neurosci. 33, 4128–4139.

Halder, S., Agorastos, D., Veit, R., Hammer, E.M., Lee, S., Varkuti, B., Bogdan, M., Rosenstiel, W., Birbaumer, N., Kubler, A., 2011. Neural mechanisms of brain-computer interface control. NeuroImage 55, 1779–1790.

Halder, S., Varkuti, B., Bogdan, M., Kubler, A., Rosenstiel, W., Sitaram, R., Birbaumer, N., 2013. Prediction of brain-computer interface aptitude from individual brain structure. Front. Hum. Neurosci. 7, 105.

Hampshire, A., Thompson, R., Duncan, J., Owen, A.M., 2011. Lateral prefrontal cortex subregions make dissociable contributions during fluid reasoning. Cereb. Cortex 21, 1–10.

Han, X., Jovicich, J., Salat, D., van der Kouwe, A., Quinn, B., Czanner, S., Busa, E., Pacheco, J., Albert, M., Killiany, R., Maguire, P., Rosas, D., Makris, N., Dale, A., Dickerson, B., Fischl, B., 2006. Reliability of MRI-derived measurements of human cerebral cortical thickness: the effects of field strength, scanner upgrade and manufacturer. NeuroImage 32, 180–194.

Hanakawa, T., Immisch, I., Toma, K., Dimyan, M.A., Van Gelderen, P., Hallett, M., 2003. Functional properties of brain areas associated with motor execution and imagery. J. Neurophysiol. 89, 989–1002.

Hetu, S., Gregoire, M., Saimpont, A., Coll, M.P., Eugene, F., Michon, P.E., Jackson, P.L., 2013. The neural network of motor imagery: an ALE meta-analysis. Neurosci. Biobehav. Rev. 37, 930–949.

Hochberg, L.R., Serruya, M.D., Friehs, G.M., Mukand, J.A., Saleh, M., Caplan, A.H., Branner, A., Chen, D., Penn, R.D., Donoghue, J.P., 2006. Neuronal ensemble control of prosthetic devices by a human with tetraplegia. Nature 442, 164–171.

Hopfinger, J.B., Buonocore, M.H., Mangun, G.R., 2000. The neural mechanisms of top-down attentional control. Nat. Neurosci. 3, 284–291.

Japkowicz, N., Stephen, S., 2002. The class imbalance problem: a systematic study. Intelligent Data Analysis. 6, pp. 429–449.

Kasahara, K., DaSalla, C.S., Honda, M., Hanakawa, T., 2015. Neuroanatomical correlates of brain-computer interface performance. NeuroImage 110, 95–100.

Kothari, S., Phan, J.H., Young, A.N., Wang, M.D., 2013. Histological image classification using biologically interpretable shape-based features. BMC Med. Imaging 13.

Krauledat, M., Grzeska, K., Sagebaum, M., Blankertz, B., Vidaurre, C., Müller, K.-R., Schröder, M., 2009. Playing pinball with non-invasive BCI. Adv. Neural Inf. Proces. Syst. 1641–1648.

Kuhn, S., Lorenz, R., Banaschewski, T., Barker, G.J., Buchel, C., Conrod, P.J., Flor, H., Garavan, H., Ittermann, B., Loth, E., Mann, K., Nees, F., Artiges, E., Paus, T., Rietschel, M., Smolka, M.N., Strohle, A., Walaszek, B., Schumann, G., Heinz, A., Gallinat, J., Consortium, I., 2014. Positive association of video game playing with left frontal cortical thickness in adolescents. PLoS One 9, e91506.

Kuperberg, G.R., Broome, M.R., McGuire, P.K., David, A.S., Eddy, M., Ozawa, F., Goff, D., West, W.C., Williams, S.C., van der Kouwe, A.J., Salat, D.H., Dale, A.M., Fischl, B., 2003. Regionally localized thinning of the cerebral cortex in schizophrenia. Arch. Gen. Psychiatry 60, 878–888.

Lakey, C.E., Berry, D.R., Sellers, E.W., 2011. Manipulating attention via mindfulness induction improves P300-based brain-computer interface performance. J. Neural Eng. 8, 025019.

Langer, N., von Bastian, C.C., Wirz, H., Oberauer, K., Jäncke, L., 2013. The effects of working memory training on functional brain network efficiency. Cortex 49, 2424–2438.

Lebedev, M., Opris, I., 2015. Brain-machine interfaces: from macro- to microcircuits. In: Casanova, M.F., Opris, I. (Eds.), Recent Advances on the Modular Organization of the Cortex. Springer, Netherlands, pp. 407–428.
Lerch, J.P., Worsley, K., Shaw, W.P., Greenstein, D.K., Lenroot, R.K., Giedd, J., Evans, A.C., 2006. Mapping anatomical correlations across cerebral cortex (MACACC) using cortical thickness from MRI. NeuroImage 31, 993–1003.
Li, P., Xu, P., Zhang, R., Guo, L., Yao, D., 2013. L1 norm based common spatial patterns decomposition for scalp EEG BCI. Biomed. Eng. Online 12, 77.
Li, M., Chen, H., Wang, J., Liu, F., Wang, Y., Lu, F., Yu, C., Chen, H., 2014. Increased cortical thickness and altered functional connectivity of the right superior temporal gyrus in left-handers. Neuropsychologia 67C, 27–34.
Liu, F., Guo, W., Fouche, J.P., Wang, Y., Wang, W., Ding, J., Zeng, L., Qiu, C., Gong, Q., Zhang, W., Chen, H., 2013a. Multivariate classification of social anxiety disorder using whole brain functional connectivity. Brain Struct. Funct.
Liu, F., Wee, C.Y., Chen, H., Shen, D., 2013b. Inter-modality relationship constrained multi-modality multi-task feature selection for Alzheimer's disease and mild cognitive impairment identification. NeuroImage 84C, 466–475.
Lohmann, G., Margulies, D.S., Horstmann, A., Pleger, B., Lepsien, J., Goldhahn, D., Schloegl, H., Stumvoll, M., Villringer, A., Turner, R., 2010. Eigenvector centrality mapping for analyzing connectivity patterns in fMRI data of the human brain. PLoS One 5, e10232.
Luckmann, H.C., Jacobs, H.I., Sack, A.T., 2014. The cross-functional role of frontoparietal regions in cognition: internal attention as the overarching mechanism. Prog. Neurobiol. 116, 66–86.
Luna, B., Padmanabhan, A., O'Hearn, K., 2010. What has fMRI told us about the development of cognitive control through adolescence? Brain Cogn. 72, 101–113.
MacDonald, D., Kabani, N., Avis, D., Evans, A.C., 2000. Automated 3-D extraction of inner and outer surfaces of cerebral cortex from MRI. NeuroImage 12, 340–356.
Madan, C.R., Singhal, A., 2012. Motor imagery and higher-level cognition: four hurdles before research can sprint forward. Cogn. Process. 13, 211–229.
Markett, S., Reuter, M., Montag, C., Voigt, G., Lachmann, B., Rudorf, S., Elger, C.E., Weber, B., 2014. Assessing the function of the fronto-parietal attention network: insights from resting-state fMRI and the attentional network test. Hum. Brain Mapp. 35, 1700–1709.
McFarland, D., McCane, L., David, S., Wolpaw, J., 1997. Spatial filter selection for EEG-based communication. Electroencephalogr. Clin. Neurophysiol. 103, 386–394.
Miller, K.J., Schalk, G., Fetz, E.E., den Nijs, M., Ojemann, J.G., Rao, R.P., 2010. Cortical activity during motor execution, motor imagery, and imagery-based online feedback. Proc. Natl. Acad. Sci. U. S. A. 107, 4430–4435.
Molinari, E., Baraldi, P., Campanella, M., Duzzi, D., Nocetti, L., Pagnoni, G., Porro, C.A., 2013. Human parietofrontal networks related to action observation detected at rest. Cereb. Cortex 23, 178–186.
Moxon, K.A., Foffani, G., 2015. Brain-machine interfaces beyond neuroprosthetics. Neuron 86, 55–67.
Muller-Gerking, J., Pfurtscheller, G., Flyvbjerg, H., 1999. Designing optimal spatial filters for single-trial EEG classification in a movement task. Clin. Neurophysiol. 110, 787–798.
Naghavi, H.R., Nyberg, L., 2005. Common fronto-parietal activity in attention, memory, and consciousness: shared demands on integration? Conscious. Cogn. 14, 390–425.
Narr, K.L., Woods, R.P., Thompson, P.M., Szeszko, P., Robinson, D., Dimtcheva, T., Gurbani, M., Toga, A.W., Bilder, R.M., 2007. Relationships between IQ and regional cortical gray matter thickness in healthy adults. Cereb. Cortex 17, 2163–2171.
Neuper, C., Scherer, R., Reiner, M., Pfurtscheller, G., 2005. Imagery of motor actions: differential effects of kinesthetic and visual-motor mode of imagery in single-trial EEG. Brain Res. Cogn. Brain Res. 25, 668–677.
Osada, T., Adachi, Y., Miyamoto, K., Jimura, K., Setsuie, R., Miyashita, Y., 2015. Dynamically allocated hub in task-evoked network predicts the vulnerable prefrontal locus for contextual memory retrieval in macaques. PLoS Biol. 13, e1002177.
Pereira, F., Mitchell, T., Botvinick, M., 2009. Machine learning classifiers and fMRI: a tutorial overview. NeuroImage 45, S199–S209.
Pisella, L., Grea, H., Tilikete, C., Vighetto, A., Desmurget, M., Rode, G., Boisson, D., Rossetti, Y., 2000. An 'automatic pilot' for the hand in human posterior parietal cortex: toward reinterpreting optic ataxia. Nat. Neurosci. 3, 729–736.
Pochon, J.B., Levy, R., Poline, J.B., Crozier, S., Lehericy, S., Pillon, B., Deweer, B., Le Bihan, D., Dubois, B., 2001. The role of dorsolateral prefrontal cortex in the preparation of forthcoming actions: an fMRI study. Cereb. Cortex 11, 260–266.
Power, J.D., Schlaggar, B.L., Lessov-Schlaggar, C.N., Petersen, S.E., 2013. Evidence for hubs in human functional brain networks. Neuron 79, 798–813.
Ptak, R., 2012. The frontoparietal attention network of the human brain: action, saliency, and a priority map of the environment. Neuroscientist 18, 502–515.
Rubinov, M., Sporns, O., 2010. Complex network measures of brain connectivity: uses and interpretations. NeuroImage 52, 1059–1069.
Sack, A.T., 2009. Parietal cortex and spatial cognition. Behav. Brain Res. 202, 153–161.
Sack, A.T., Schuhmann, T., 2012. Hemispheric differences within the fronto-parietal network dynamics underlying spatial imagery. Front. Psychol. 3, 214.
Sato, J.R., Salum, G.A., Gadelha, A., Vieira, G., Zugman, A., Picon, F.A., Pan, P.M., Hoexter, M.Q., Anes, M., Moura, L.M., Del'Aquilla, M.A., Crossley, N., Amaro Junior, E., McGuire, P., Lacerda, A.L., Rohde, L.A., Miguel, E.C., Jackowski, A.P., Bressan, R.A., 2015. Decreased centrality of subcortical regions during the transition to adolescence: a functional connectivity study. NeuroImage 104, 44–51.
Scolari, M., Seidl-Rathkopf, K.N., Kastner, S., 2015. Functions of the human frontoparietal attention network: evidence from neuroimaging. Curr. Opin. Behav. Sci. 1, 32–39.
Sharp, D.J., Scott, S.K., Wise, R.J.S., 2004. Monitoring and the controlled processing of meaning: distinct prefrontal systems. Cereb. Cortex 14, 1–10.
Shaw, P., Malek, M., Watson, B., Greenstein, D., de Rossi, P., Sharp, W., 2013. Trajectories of cerebral cortical development in childhood and adolescence and adult attention-deficit/hyperactivity disorder. Biol. Psychiatry 74, 599–606.
Sirigu, A., Duhamel, J.R., Cohen, L., Pillon, B., Dubois, B., Agid, Y., 1996. The mental representation of hand movements after parietal cortex damage. Science 273, 1564–1568.
Sowell, E.R., Thompson, P.M., Leonard, C.M., Welcome, S.E., Kan, E., Toga, A.W., 2004. Longitudinal mapping of cortical thickness and brain growth in normal children. J. Neurosci. 24, 8223–8231.
Sporns, O., 2013a. Making sense of brain network data. Nat. Methods 10, 491–493.
Sporns, O., 2013b. Structure and function of complex brain networks. Dialogues Clin. Neurosci. 15, 247–262.
Thomas, J.B., Brier, M.R., Ortega, M., Benzinger, T.L., Ances, B.M., 2015. Weighted brain networks in disease: centrality and entropy in human immunodeficiency virus and aging. Neurobiol. Aging 36, 401–412.
Toro, R., Fox, P.T., Paus, T., 2008. Functional coactivation map of the human brain. Cereb. Cortex 18, 2553–2559.
Tuladhar, A.M., Reid, A.T., Shumskaya, E., de Laat, K.F., van Norden, A.G., van Dijk, E.J., Norris, D.G., de Leeuw, F.E., 2015. Relationship between white matter hyperintensities, cortical thickness, and cognition. Stroke 46, 425–432.
Vendetti, Michael S., Bunge, Silvia A., 2014. Evolutionary and developmental changes in the lateral frontoparietal network: a little goes a long way for higher-level cognition. Neuron 84, 906–917.
Vidaurre, C., Blankertz, B., 2010. Towards a cure for BCI illiteracy. Brain Topogr. 23, 194–198.
Voss, P., Zatorre, R.J., 2015. Early visual deprivation changes cortical anatomical covariance in dorsal-stream structures. NeuroImage 108, 194–202.
Wendelken, C., Bunge, S.A., Carter, C.S., 2008. Maintaining structured information: an investigation into functions of parietal and lateral prefrontal cortices. Neuropsychologia 46, 665–678.
Wendelken, C., O'Hare, E.D., Whitaker, K.J., Ferrer, E., Bunge, S.A., 2011. Increased functional selectivity over development in rostrolateral prefrontal cortex. J. Neurosci. 31, 17260–17268.
Xu, P., Yang, P., Lei, X., Yao, D., 2011. An enhanced probabilistic LDA for multi-class brain computer interface. PLoS One 6, e14634.
Zacks, J.M., 2008. Neuroimaging studies of mental rotation: a meta-analysis and review. J. Cogn. Neurosci. 20, 1–19.
Zalesky, A., Fornito, A., Bullmore, E.T., 2010. Network-based statistic: identifying differences in brain networks. NeuroImage 53, 1197–1207.
Zanto, T.P., Gazzaley, A., 2013. Fronto-parietal network: flexible hub of cognitive control. Trends Cogn. Sci. 17, 602–603.
Zhang, R., Xu, P., Guo, L., Zhang, Y., Li, P., Yao, D., 2013a. Z-score linear discriminant analysis for EEG based brain-computer interfaces. PLoS One 8, e74433.
Zhang, R., Xu, P., Liu, T., Zhang, Y., Guo, L., Li, P., Yao, D., 2013b. Local temporal correlation common spatial patterns for single trial EEG classification during motor imagery. Comput. Math Methods Med. 2013, 7.
Zhang, R., Xu, P., Chen, R., Li, F., Guo, L., Li, P., Zhang, T., Yao, D., 2015a. Predicting inter-session performance of SMR-based brain-computer interface using the spectral entropy of resting-state EEG. Brain Topogr.
Zhang, R., Yao, D., Valdes-Sosa, P.A., Li, F., Li, P., Zhang, T., Ma, T., Li, Y., Xu, P., 2015b. Efficient resting-state EEG network facilitates motor imagery performance. J. Neural Eng. 12, 066024.
Zhou, D., Lebel, C., Treit, S., Evans, A., Beaulieu, C., 2015. Accelerated longitudinal cortical thinning in adolescence. NeuroImage 104, 138–145.
Zich, C., Debener, S., Kranczioch, C., Bleichner, M.G., Gutberlet, I., De Vos, M., 2015. Real-time EEG feedback during simultaneous EEG-fMRI identifies the cortical signature of motor imagery. NeuroImage 114, 438–447.
Zielinski, B.A., Prigge, M.B., Nielsen, J.A., Froehlich, A.L., Abildskov, T.J., Anderson, J.S., Fletcher, P.T., Zygmunt, K.M., Travers, B.G., Lange, N., Alexander, A.L., Bigler, E.D., Lainhart, J.E., 2014. Longitudinal changes in cortical thickness in autism and typical development. Brain 137, 1799–1812.
Zuo, X.N., Ehmke, R., Mennes, M., Imperati, D., Castellanos, F.X., Sporns, O., Milham, M.P., 2012. Network centrality in the human functional connectome. Cereb. Cortex 22, 1862–1875.